Supplementary Methods

Cell culture and chemicals

Human and mouse breast cancer cell lines were obtained from American Type Culture Collection. Normal human mammary epithelial cells (HMECs) were purchased from Clonetics (Walkersville, MD). Cell proliferation was assessed by the 3-(4,5-dimethylthiazol-2-yl)-2,5-diphenyltetrazolium (MTT) assay. Soft agar colony formation assay was performed by using 0.3 % agar in complete medium with cells as the feeder layer, and 0.6 % agar in complete medium as the bottom layer. 3D Matrigel culture was performed using Matrigel matrix (BD Biosciences). Akt inhibitor AI-IV (a benzimidazole compound) (1), BMS-345541 (IKK inhibitor III), Bay 11-7082 and JSH-23 (NF-κB Activation Inhibitor II) were purchased from Calbiochem (Gibbstown, NJ). Diamide, buthionine sulfoximine (BSO) and N-Acetyl-L-cysteine (NAC) were purchased from Sigma (St Louis, MO). The Trx-1 inhibitor PX-12 was kindly provided by ProlX Pharmaceuticals/Oncothyreon Inc.

Gene expression analysis

Control and TXNL2-KD MDA-MB 231 cells were harvested and total RNA was extracted using the RNeasy Mini kit (Qiagen) according to the manufacturer's instructions. RNA quantity and purity were assessed by measurement of OD260/280 using a NanoDrop® ND-1000 spectrophotometer. The quality was verified by the integrity of 28S and 18S rRNA using the Agilent Total RNA Nano chip assay on a Model 2100 Bioanalyzer (Agilent Technologies, Santa Clara, CA). The intensity of the 28S band should be twice the intensity of the 18S band. Gene expression profiling was conducted using the Human OneArray™ (Phalanx Biotech, Palo Alto, CA) containing over 30,000 sixty-mer polynucleotide probes with each probe mapped to the

latest draft of the human genome (GoldenPath) printed on standard 1-in. x 3-in. glass slides. Analysis was performed according to the manufacturer's recommendations. Two technical repetitions were performed. After hybridization, arrays were scanned using GenePix 4000B (Axon Instruments, Union City, CA) and analyzed with GenePix Pro 6.0 (Axon Instruments, Union City, CA) to obtain gene expression ratios. Transformed data were normalized using the Lowess procedure (5). The normalized data were used for clustering analysis. Clustering analysis was performed using Genespring GX 10.0 software (Agilent Technologies) to provide a graphical display of the expression patterns.

Cell migration and invasion assay

Cell migration ability was analyzed by a transwell chamber assay. Cell invasion assays were performed using BD BioCoat™ Matrigel™ Invasion Chambers. 10 % FCS was used as the chemoattractant. Cells on the lower surface of the insert were fixed and stained followed by counting under a light microscope.

Immunofluorescence staining

Cells were fixed with 4 % formaldehyde and then permeabilized with PBS containing 0.2 % Triton X-100. Slides were blocked by 5 % BSA and incubated with a primary antibody at room temperature for 1 h. Then, FITC or TRITC conjugated secondary antibody was added to incubate for another 30 min. For F-actin staining, cells were fixed and then incubated with Alexa Fluor 555® phalloidin (Invitrogen) for 30 min. Slides were washed by PBS, mounted in DAPI, and observed under microscope. As a negative control, primary specific antibodies were replaced with a control mouse IgG.

Wound healing assay

Control shRNA and TXNL2 shRNA MDA-MB-231 cells were plated in 6-well plates and grown to confluency. A wound area was generated by scraping cells with a 200 μl pipette tip across the entire diameter of the dish and extensively rinsed with the medium to remove all cellular debris. Low-serum DMEM with mitomycin (2 μg/ml) was then added to inhibit cell proliferation during the experiment and the closing of the wound was observed at different time points.

Reverse transcription-PCR (RT-PCR)

Total RNA was isolated from different cell lines using RNeasy Mini Kit (Qiagen, Valencia, CA). Equal amount of RNA was reverse transcribed into cDNA by using SuperScript III system (Invitrogen, Carlsbad, CA). Primers used for all the genes are listed in Supplementary Table 1.

Western blotting

Whole cell lysates were harvested using cell lysis buffer supplemented with a protease inhibitor cocktail (Sigma). The nuclear and cytosol extracts were isolated using the nuclear extract kit (Active Motif, Carlsbad, CA) according to the manufacturer's instructions. Signals were visualized using enhanced chemiluminescence (Pierce). Antibodies against α-catenin, γ-catenin, Lamin A/C, Grx-1, and Trx-1 were purchased form Santa Cruz Biotechnology (Santa Cruz, CA). Antibodies against p-Akt (Ser473), Akt, p-p65 (Ser536), p-IκBα (Ser32), IκBα, and IKKβ were obtained from Cell Signaling (Danvers, MA) and used at a 1: 1000 dilution. Antibodies against E-cadherin, β-catenin, and vimentin were purchased from BD Biosciences. Antibodies against p65, p50, p52, and RelB were obtained from Active Motif. Anti-GSH was purchased from

Virogen (Watertown, MA). Anti-β and α-Smooth Muscle actin (α-SMA) (Sigma) were used at a 1: 5000 dilution.

Glutathione assay

Intracellular glutathione was measured by using the Glutathione assay kit (Cayman Chemical Company, Ann Arbor, MI). Briefly, for total glutathione, cells were harvested and sonicated in ice cold buffer (50 mM MES). The same amount of cleared cell lysates was used after deproteination with MPA reagent. Measurement of GSSG was accomplished by first derivatizing GSH with 2-vinylpridine.

***In vitro* kinase assay**

For IKK kinase assay, an equal amount of cell lysates was incubated with IKKβ (1: 50) overnight at 4 °C, followed by adding 20 µl sepharose A/G 1 h at 4 °C. The pellet was washed twice by lysis buffer and twice with kinase buffer (Cell signaling), then incubated with 50 µl kinase assay buffer and 1 µg reconstituted IκBα protein (Santa Cruz) at room temperature for 30 min. The reaction was terminated by adding SDS sample buffer, and then heated for 5 min at 100 °C. The activity of Rac1 and RhoA small GTPases was examined by G-LISA activation kit. Ras activity was examined by Raf-RBD pull-down assay. The kits were obtained from Cytoskeleton (Denver, CO) and the procedure was followed according to the manufacture's instructions.

Transfection of cells with TXNL2 siRNA and mouse TXNL2

Human TXNL2 siRNAs (Santa Cruz Biotech, Santa Cruz, CA) were transiently transfected into breast cancer cells for different time periods. These siRNA sequences are shown in

Supplementary Table 2. TXNL2 levels were examined by RT-PCR and western blotting. ROS levels and NF-κB activity were measured using FACS and luciferase reporter assays. To further rule out the off-target effects of human TXNL2 shRNA, a full-length mouse TXNL2 cDNA was inserted in the vector pcDNA3.1 (Invitrogen) and transfected into TXNL2 shRNA MDA-MB-231 cells. Stable clones were obtained by G418 selection. Of note, TXNL2-KD cells are puromycin resistant.

***In vivo* tumorigenesis and metastasis**

1×10^7 cells were injected into the mammary fat pads of 4- to 5-week-old female severe combined immunodeficient (SCID) mice. The growth of primary tumors was monitored every 3 days by measuring tumor diameters. Tumor length (L) and width (W) were measured and tumor volume was calculated by the equation: volume = $(W^2 \times L)/2$. Mice were sacrificed 37 days after injection. To produce experimental lung metastasis, 2×10^6 cells were injected into the lateral tail veins of 4-to 5-week-old female SCID mice. After 6 weeks, the mice were sacrificed under anesthesia. Lungs were stained with 15 % black India ink as described previously (6). Visible lung surface macrometastatic appeared as white spots and were counted using a dissecting microscope. Lungs were collected and fixed in 10 % formalin. For tissue morphology evaluation, hematoxylin and eosin (H&E) staining were performed on sections from embedded samples.

Survival Analysis

Raw data files from a publicly available 192-sample gene expression microarray dataset (Affymetrix U133 2.0) derived from primary human breast cancer samples having known metastasis profiles were analyzed using Genespring GX 10.0 software (Agilent Technologies)

(7). Raw data files from a 189-sample dataset (8) and a 159-sample dataset (9) (Affymetrix U133A) derived from primary human breast cancer samples having known clinical outcome measures were similarly analyzed using the above software. Signal intensities were obtained using the Robust Multi-chip Averaging (RMA) algorithm to perform background correction, normalization and summarization of probe-level raw data. All values underwent baseline transformation to median of all samples in a particular dataset on a gene/probeset basis. Array quality control was performed using 3D Principal Component Analysis (PCA) scores in the PCA plot, Internal Controls comprising of 3'/5' ratios for a set of specific housekeeping gene probe sets, and Hybridization Controls. Probes were filtered based on signal intensity values so that values between 20.0 and 100.0 percentiles were retained. The mRNA level (mean $\log_2$ signal intensity) for TXNL2 was determined for each sample and the potential association between TXNL2 expression and the occurrence of metastasis to the lung and/or brain was examined in the 192-sample dataset. The Wilcoxon rank sum test was used to assess statistical significance for this comparison. Lung-specific and brain-specific metastasis-free survival was also examined in the same dataset using the log-rank test and survival plots were created using Kaplan-Meier methods. Prognostic significance of TXNL2 in predicting recurrence-free survival and distant metastasis-free survival in breast cancer patients was examined in the Sotiriou et al. (8) microarray dataset. Prognostic significance of TXNL2 in predicting disease-specific survival and overall survival in breast cancer patients was examined in the Pawitan et al. (9) microarray dataset. Survival plots for these analyses were also created using Kaplan-Meier methods.

References

1. Kau, T.R., Schroeder, F., Ramaswamy, S., Wojciechowski, C.L., Zhao, J.J., Roberts, T.M., Clardy, J., Sellers, W.R., and Silver, P.A. 2003. A chemical genetic screen identifies inhibitors of regulated nuclear export of a Forkhead transcription factor in PTEN-deficient tumor cells. *Cancer Cell* 4:463-476.
2. Chen, X., Leung, S.Y., Yuen, S.T., Chu, K.M., Ji, J., Li, R., Chan, A.S., Law, S., Troyanskaya, O.G., Wong, J., et al. 2003. Variation in gene expression patterns in human gastric cancers. *Mol Biol Cell* 14:3208-3215.
3. Dyrskjot, L., Kruhoffer, M., Thykjaer, T., Marcussen, N., Jensen, J.L., Moller, K., and Orntoft, T.F. 2004. Gene expression in the urinary bladder: a common carcinoma in situ gene expression signature exists disregarding histopathological classification. *Cancer Res* 64:4040-4048.
4. Pyeon, D., Newton, M.A., Lambert, P.F., den Boon, J.A., Sengupta, S., Marsit, C.J., Woodworth, C.D., Connor, J.P., Haugen, T.H., Smith, E.M., et al. 2007. Fundamental differences in cell cycle deregulation in human papillomavirus-positive and human papillomavirus-negative head/neck and cervical cancers. *Cancer Res* 67:4605-4619.
5. Yang, Y.H., Dudoit, S., Luu, P., Lin, D.M., Peng, V., Ngai, J., and Speed, T.P. 2002. Normalization for cDNA microarray data: a robust composite method addressing single and multiple slide systematic variation. *Nucleic Acids Res* 30:e15.
6. Safina, A., Vandette, E., and Bakin, A.V. 2007. ALK5 promotes tumor angiogenesis by upregulating matrix metalloproteinase-9 in tumor cells. *Oncogene* 26:2407-2422.

7. Bos, P.D., Zhang, X.H., Nadal, C., Shu, W., Gomis, R.R., Nguyen, D.X., Minn, A.J., van de Vijver, M.J., Gerald, W.L., Foekens, J.A., et al. 2009. Genes that mediate breast cancer metastasis to the brain. *Nature* 459:1005-1009.

8. Sotiriou, C., Wirapati, P., Loi, S., Harris, A., Fox, S., Smeds, J., Nordgren, H., Farmer, P., Praz, V., Haibe-Kains, B., et al. 2006. Gene expression profiling in breast cancer: understanding the molecular basis of histologic grade to improve prognosis. *J Natl Cancer Inst* 98:262-272.

9. Pawitan, Y., Bjohle, J., Amler, L., Borg, A.L., Egyhazi, S., Hall, P., Han, X., Holmberg, L., Huang, F., Klaar, S., et al. 2005. Gene expression profiling spares early breast cancer patients from adjuvant therapy: derived and validated in two population-based cohorts. *Breast Cancer Res* 7:R953-964.

Supplemental Table 1. Primers of RT-PCR

	Forward	Reverse
IκBα	5'-actcctgttgaagtgtgggg-3'	5'-gctcgtcctctgtgaactcc-3'
RelB	5'-ccctgaagaaccatcaggaa-3'	5'-aggtacgtgaaaggcaatgg-3'
BCL2A1	5'-ggctcaggactatctgcagtgcg-3'	5'-agccattttcccagcctccgt-3'
CRADD	5'-tgcagacggagaaatggaggcca-3'	5'-ccactcagggcccagcctct-3'
IL-1β	5'-acgctccgggactcacagca-3'	5'-ccctcccaggaagacgggca-3'
A20	5'-gggcccggagaggtgttgga-3'	5'-cgtgctgaacagcgccttcct-3'
KISS-1	5'-tgaactcactggtttcttggcagc-3'	5'-agttccagttgtagttcggcaggt-3'
MMP-1	5'-attggagtagcaagaggctgggaa-3'	5'-tcagtgaggacaaactgagccaca-3'
TIMP-3	5'-acctgctgacaggtcgcgtct-3'	5'-gctcagcgggaagggaggga-3'
SNAIL	5'-cctccctgtcagatgaggac-3'	5'-ccaggctgaggtattccttg-3'
SLUG	5'-agcgaactggacacacatac-3'	5'-tctagactgggcatcgcag-3'
TWIST	5'-ggagtccgcagtcttacgag-3'	5'-tctggaggacctggtagagg-3'
E-cad	5'-tgcccagaaaatgaaaaagg-3'	5'-gtgtatgtggcaatgcgttc-3'
β-actin	5'-caggcaccagggcgtgatgg-3'	5'-ctgtagccgcgctcggtgag-3'

Supplemental Table 2. Sequences of human TXNL2-specific siRNAs

	sense	anti-sense
siRNA-1	CGAAGUUAUGGCAGAGUUAtt	UAACUCUGCCAUAACUUCGtt
siRNA-2	CUGUGAUGCUCUUUAUGAAtt	UUCAUAAAGAGCAUCACAGtt

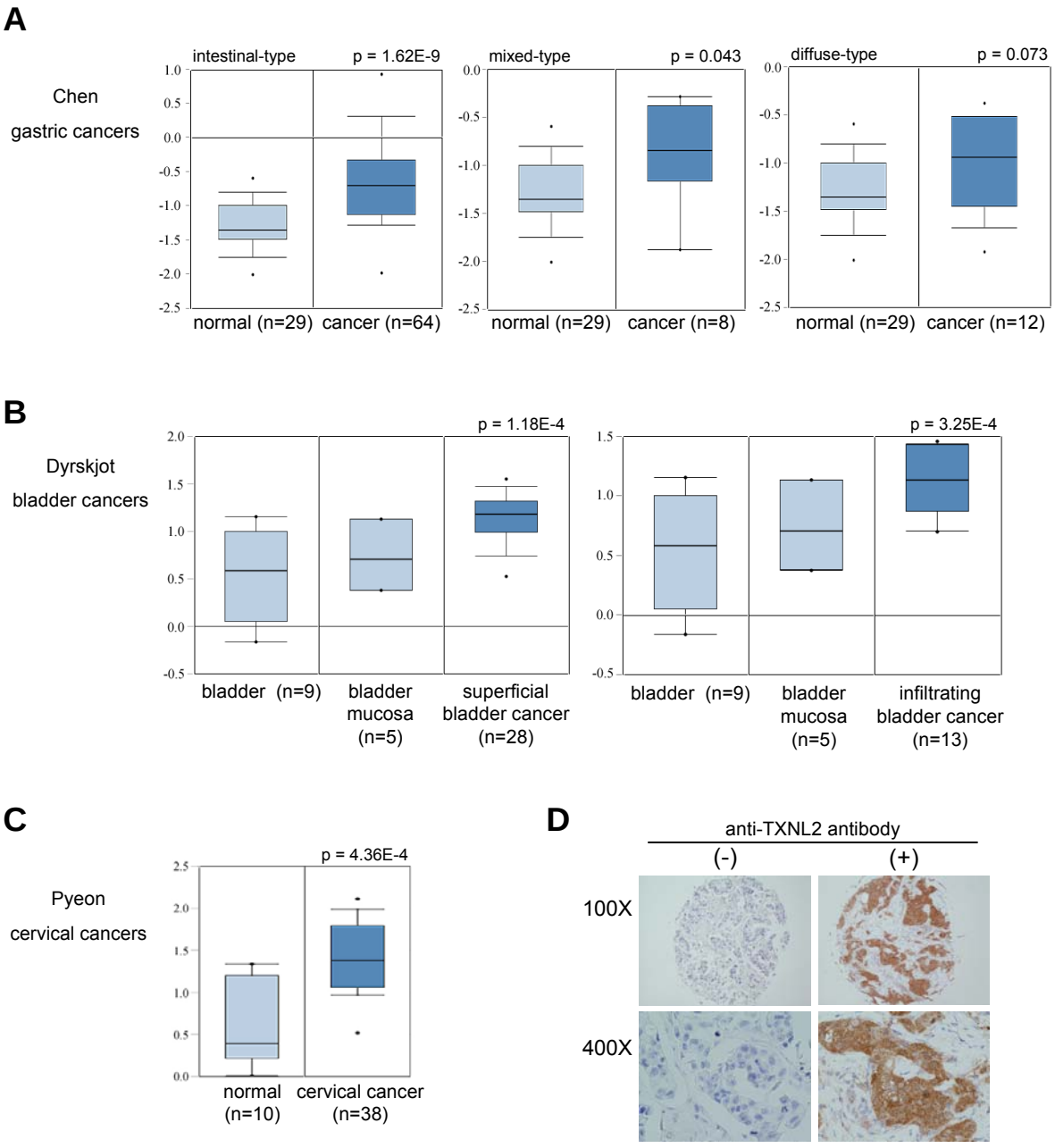

Figure S1

Analysis of TXNL2 expression in human cancers. Representative plotted data from the Oncomine database show TXNL2 mRNA expression in gastric **(A)** , bladder **(B)** , and cervical **(C)** cancer/normal tissues. **(D)** Representative IHC staining of human breast cancers using normal mouse IgG (left panel) and a mouse monoclonal anti-TXNL2 antibody (right panel) is shown.

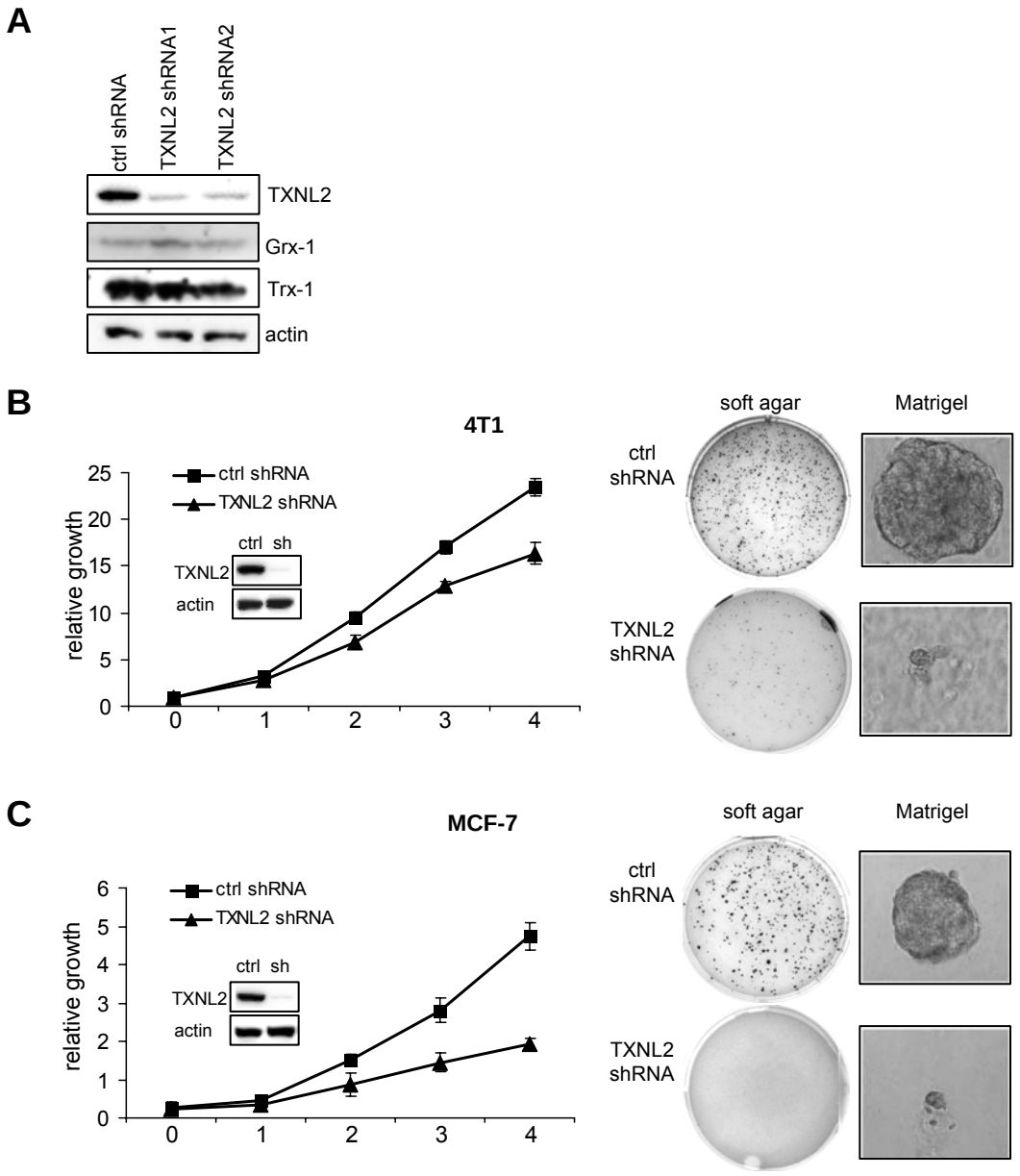

Figure S2

TXNL2 knockdown inhibits cell growth. (A) The effectiveness and specificity of two TXNL2 shRNAs were indicated by immunoblotting. Growth of control and TXNL2-KD 4T1 **(B)** and MCF-7 **(C)** breast cancer cells in monolayer culture, soft agar and 3-D Matrigel are shown. magnification: × 200.

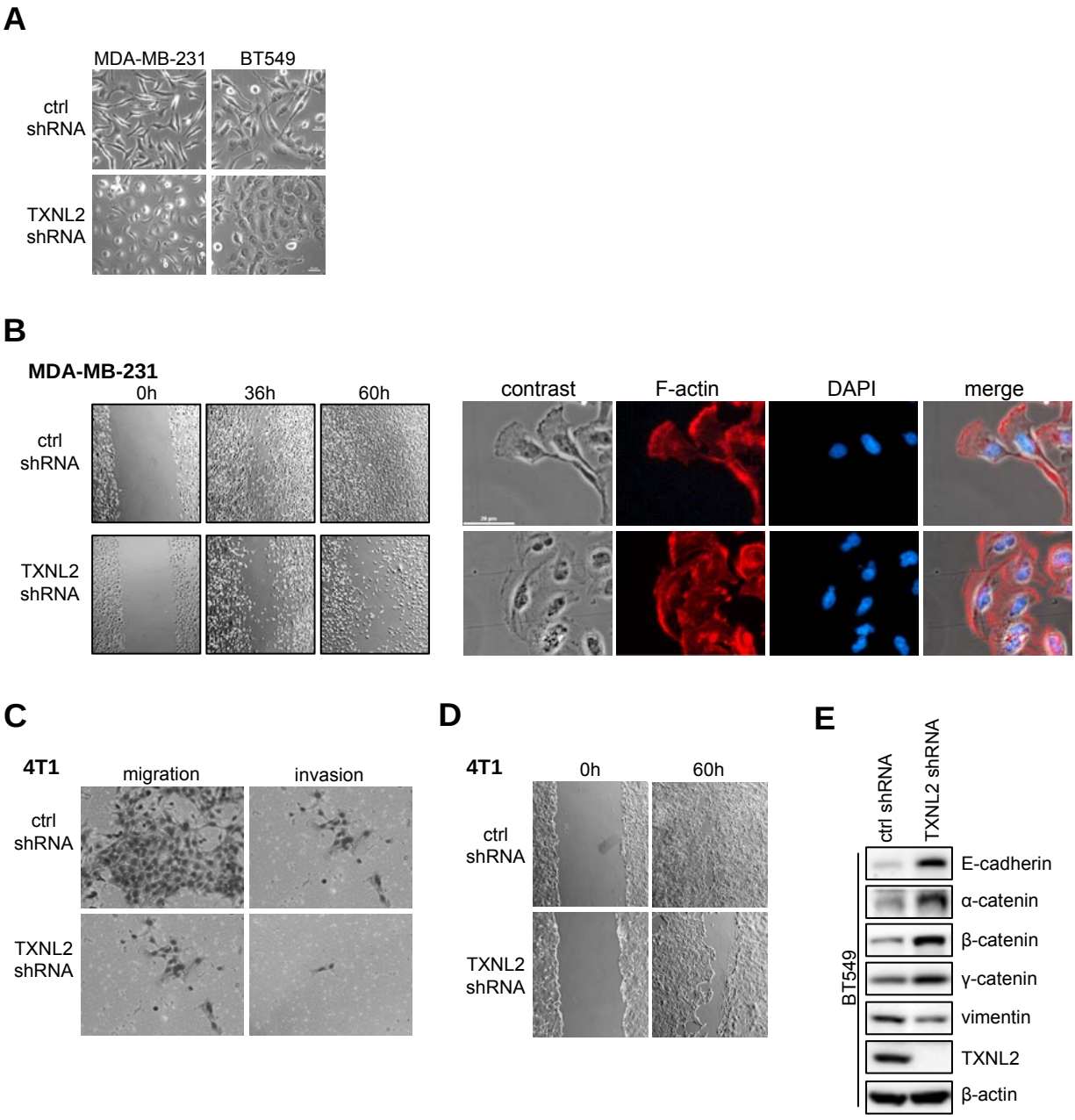

Figure S3

TXNL2 deficiency impairs cell migration and invasion. (A) Morphologies of control and TXNL2-KD MDA-MB-231 and BT549 were revealed by microscopy (magnification: × 200). **(B)** Wound healing assays (left panel) were conducted. Control and TXNL2 shRNA MDA-MB-231 cells were grown in 6-well plates until confluency and then were scratched with a 200 µl tip. Wound healing process was observed at different time points after scratching (magnification: ×100). F-actin staining shows stress fibers at the wound edge in control and TXNL2-KD MDA-MB-231 cells (right panel). Nuclei were stained by DAPI. **(C)** *In vitro* migration and invasion assays in control and TXNL2-KD 4T1 cells. **(D)** Wound healing assays using control and TXNL2-KD 4T1 cells (magnification: × 100). **(E)** EMT markers in control and TXNL2-KD BT549 cells were measured by immunoblotting.

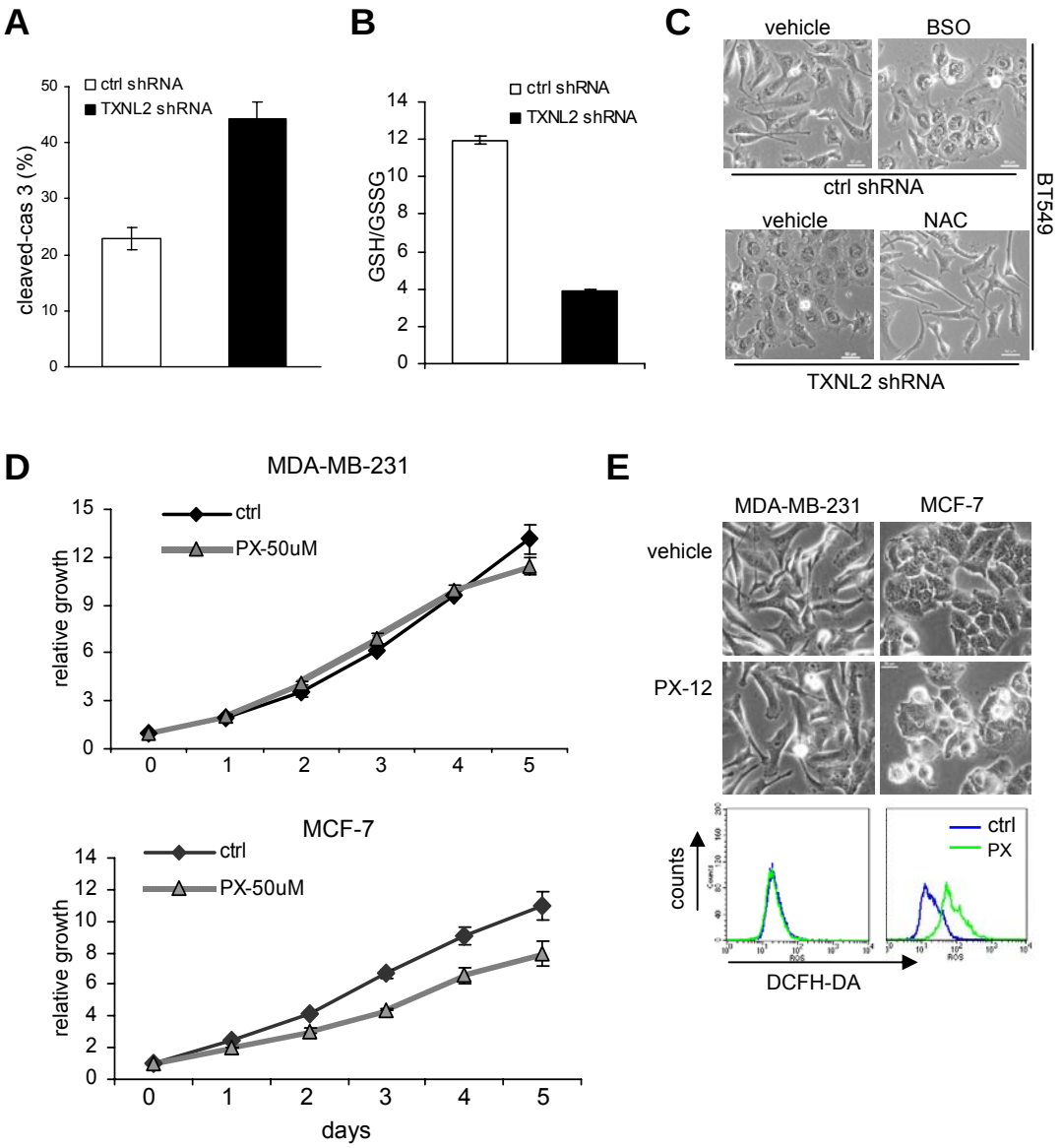

Figure S4

TXNL2 deficiency induces ROS and apoptosis. (A) Cleaved-caspase 3 (cleaved-cas 3)-positive cells in control and TXNL2-KD MDA-MB-231 cells were measured by flow cytometry. Percentages of the positive cells are plotted. **(B)** GSH/GSSG ratio was measured by the glutathione assays in control and TXNL2-KD MDA-MB-231 cells. **(C)** Changes in the morphology of control and TXNL2 shRNA BT549 cells after treating with BSO or NAC. Bar: 50 µm. **(D)** Growth curves show MDA-MD-231 and MCF-7 cells treated with or without the Trx-1 inhibitor PX-12. Data represent three independent experiments. **(E)** PX-12 (50 µM) did not induce morphological changes in MDA-MB-231 and MCF-7 cells. Intracellular ROS levels in MCF-7 cells were measured using DCFH-DA in control and PX-12 treatment groups. Bar: 50 µm.

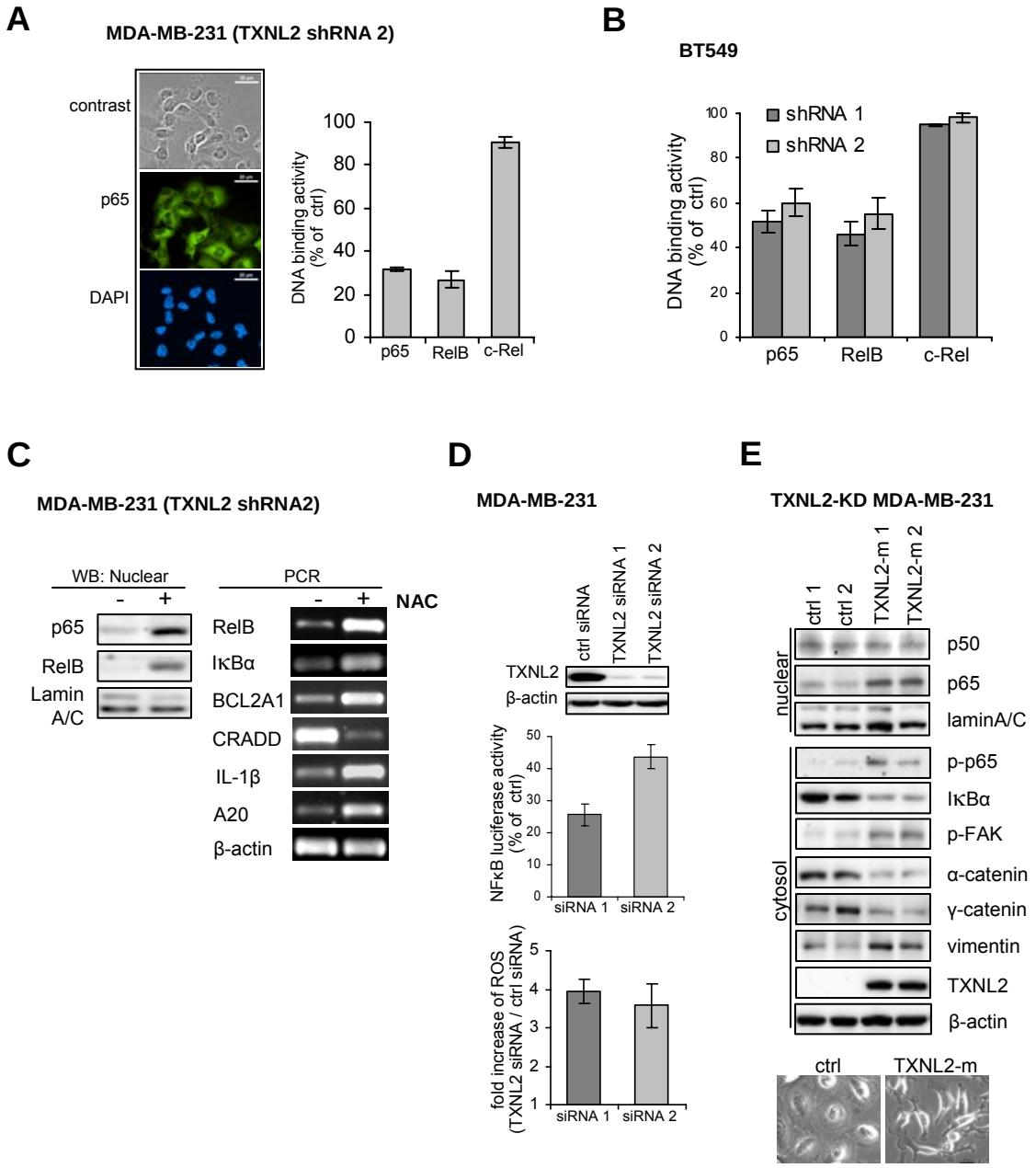

Figure S5

TXNL2 deficiency impairs p65 activity. (A) Nuclear localization of p65 in TXNL2 shRNA2 MDA-MB-231 cells was visualized by indirect immunofluorescence staining. DAPI (blue) was used to show nuclei. Relative DNA binding activities (vs. control) of p65, RelB, and c-Rel were measured by TransAM DNA-binding ELISA. **(B)** Relative DNA binding activities (vs. control) of p65, RelB, and c-Rel in control and TXNL2 shRNA BT549 cells were measured by ELISA. Data represent mean ± SD of three experiments. **(C)** TXNL2 shRNA2 MDA-MB-231 cells were treated with NAC for 6 h. Nuclear localization of p65 and RelB was examined by immunoblotting. NF-κB-regulated genes were measured by semi-quantitative RT-PCR. **(D)** TXNL2 expression in MDA-MB-231 cells was inhibited by siRNA transfection. NF-κB activity was detected by luciferase reporter assays and ROS levels were measured by FACS. **(E)** Mouse TXNL2 cDNA (TXNL2-m) was stably transfected into TXNL2-KD MDA-MB-231 cells. Expression of NF-κB components and EMT markers was examined by immunoblotting. Morphologies of control and TXNL2-m-expressing TXNL2-KD MDA-MB-231 are shown (bottom).

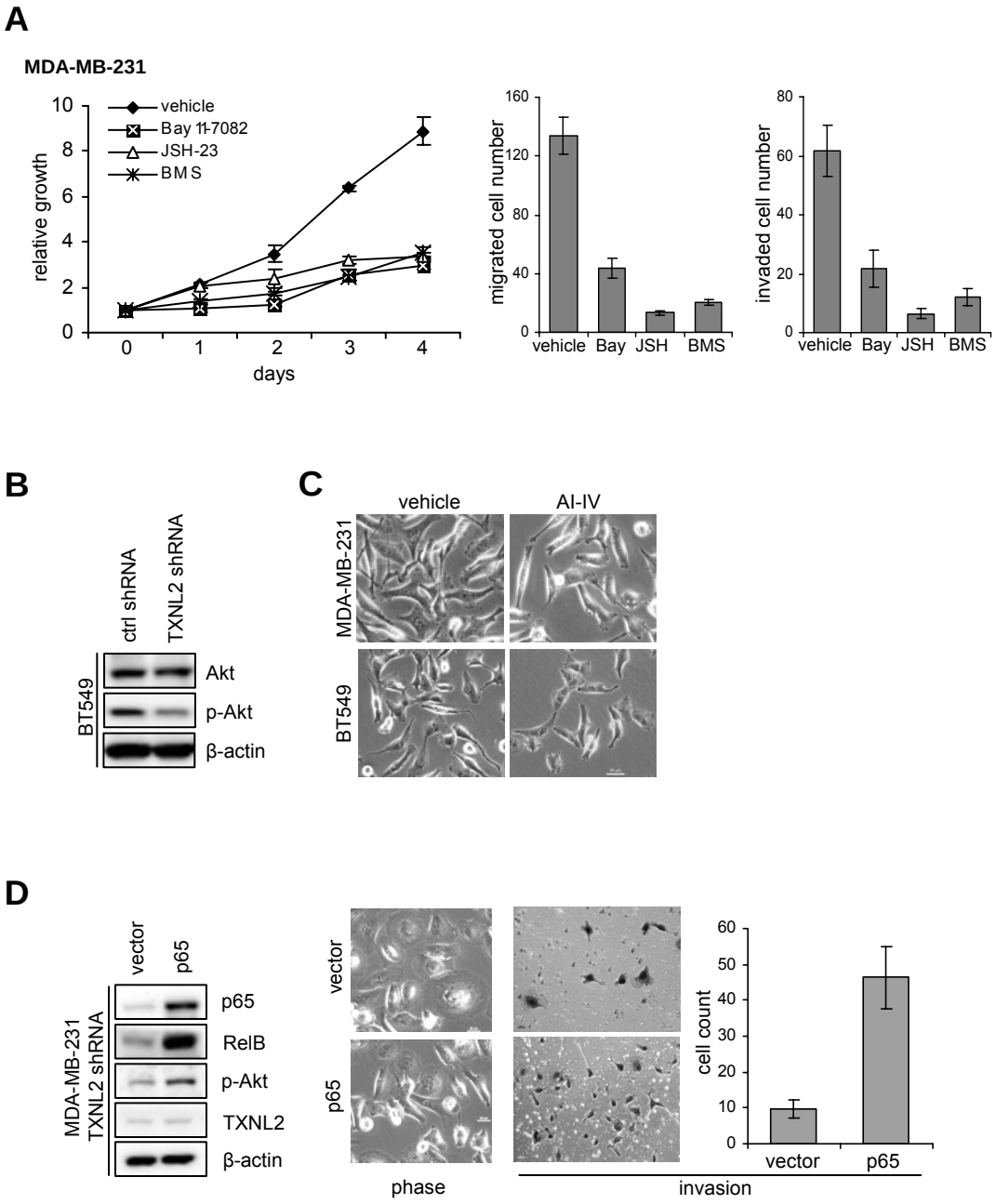

Figure S6

NF-κB mediates the effects of TXNL2 on cell function and Akt activity. (A) Suppressing NF-κB activity with Bay 11-7082, JSH-23, or BMS-345541 inhibited the growth, migration, and invasion of MDA-MB-231 cells. **(B)** Akt activation in control and TXNL2-KD BT549 cells was measured by immunoblotting. **(C)** Akt inhibition by AI-IV treatment did not reverse fibroblast morphology. Bar: 50 μm. **(D)** Overexpression of p65 in TXNL2-KD MDA-MB-231 cells rescued p-Akt and RelB levels shown by immunoblotting (left), fibroblast morphology (middle), and cell invasion capability (right).